Key-lock mechanism in nematic colloidal dispersions

N. M. Silvestre,[1] P. Patrício,[1,2] and M. M. Telo da Gama[1]
[1]*Departamento de Física da Faculdade de Ciências and Centro de Física Teórica e Computacional Universidade de Lisboa, Avenida Professor Gama Pinto 2, P-1649-003 Lisboa Codex, Portugal*
[2]*Instituto Superior de Engenharia de Lisboa, Rua Conselheiro Emídio Navarro 1, P-1949-014 Lisboa, Portugal*
(Received 4 December 2003; revised manuscript received 10 March 2004; published 16 June 2004)

We consider the interaction between two-dimensional nematic colloids and planar or sculpted walls. The elastic interaction between colloidal disks and flat walls, with homeotropic boundary conditions, is always repulsive. These repulsions may be turned into strong attractions at structured or sculpted walls, with cavities that match closely the shape and size of the colloids. This key-lock mechanism is analyzed in detail for colloidal disks and spherocylindrical cavities of various length to depth ratios, by minimizing the Landau–de Gennes free energy functional of the nematic orientational order parameter. We find that the attractions occur only for walls with cavities within a small range of the colloidal size and a narrow range of orientations with respect to the cavity's symmetry axis.

DOI: 10.1103/PhysRevE.69.061402 PACS number(s): 82.70.Dd, 61.30.Hn, 61.30.Jf

I. INTRODUCTION

In the last ten years, there has been continued interest in colloidal dispersions in nematics and other liquid crystalline phases (LCs) owing to their novel, complex behavior [1]. The behavior of spherical isotropic particles in a nematic matrix depends upon (i) the elastic constants of the nematic, (ii) the size of the particle, and (iii) the boundary conditions at the particle and at the container, including the anchoring energy of the nematogenic molecules and possibly additional (generic) surface tension effects. All of these contributions are temperature dependent and their combination leads to complex anisotropic long-ranged colloidal interactions [2–4]. These were reported to lead to a variety of novel self-organized colloidal structures, such as linear chains [5,6], periodic lattices [7], anisotropic clusters [8], and cellular structures [9] that are stabilized, in general, by topological defects.

More recently, two-dimensional (2D) inverted nematic emulsions were also studied and similar behavior has been found [10–14]. In particular, Landau–de Gennes (LdG) theory predicts that the stable configuration for a colloidal disk, with strong homeotropic anchoring, is always a pair of $1/2$ charge topological defects [15] and thus the long-range interaction between 2D colloids is quadrupolar for any sized particles [14].

The interactions between colloids and the nematic-isotropic (NI) interface were also investigated [16,17]. These include specific contributions from the liquid crystal matrix due to distortion of the director field close to the particles and/or the interface, and a generic contribution due to wetting and surface tension effects. At equilibrium, a strong distortion of the planar interfacial region was observed, with the interface bending around to wrap the colloid. The effective colloid-interface interaction was found to be rather complex and a simple scaling analysis for a flat interface was shown to fail badly [17].

At the same time technological advances allowed the controlled fabrication of micropatterned and structured surfaces, on the nanometer to the micrometer scales [18]. The interplay between surface geometry and orientational order required to understand the phenomenology of LCs on substrates patterned on these length scales is however largely unexplored. In this article we embark on a systematic investigation of the effects of geometry and orientational order on the interaction between colloids and solid surfaces. In particular, we investigate the interaction between 2D colloids and hard surfaces, ranging from flat to structured on the colloidal scale. We study the interaction between one disk and flat as well as structured walls, using the method of images and numerical minimization the LdG free energy. For a single cavity, sculpted on a flat surface, we find that the flat wall repulsion may be turned into a rather strong attraction, as a result of the interplay between geometry and orientational order. This effect occurs at cavities with sizes in the colloidal range resembling the so-called *key-lock* mechanism.

In Sec. II, we review briefly the Landau–de Gennes theory and in Sec. III we present the results for the interaction between one disk and a flat wall. In Sec. IV we consider the interaction of colloidal disks with cavities sculpted on flat walls. We investigate the effects of the size and shape of the cavity and of the colloidal orientation with respect to the cavity's symmetry axis. Finally, in Sec. V we summarize our results and make some concluding remarks.

II. LANDAU–DE GENNES FUNCTIONAL

In what follows we consider a two-dimensional nematic liquid crystal. On average, the molecules are aligned along one common direction described by the director **n** and the tensor order parameter is defined as $Q_{\alpha\beta}(\mathbf{r})=Q(\mathbf{r})\times[n_\alpha(\mathbf{r})n_\beta(\mathbf{r})-\delta_{\alpha\beta}/2]$ [19]. In the situations to be investigated, the distances over which significant variations of $Q_{\alpha\beta}$ occur are much larger than molecular dimensions. Thus density variations are neglected. The free energy density is then written in terms of invariants of **Q** and its derivatives and is known as the Landau–de Gennes free energy,

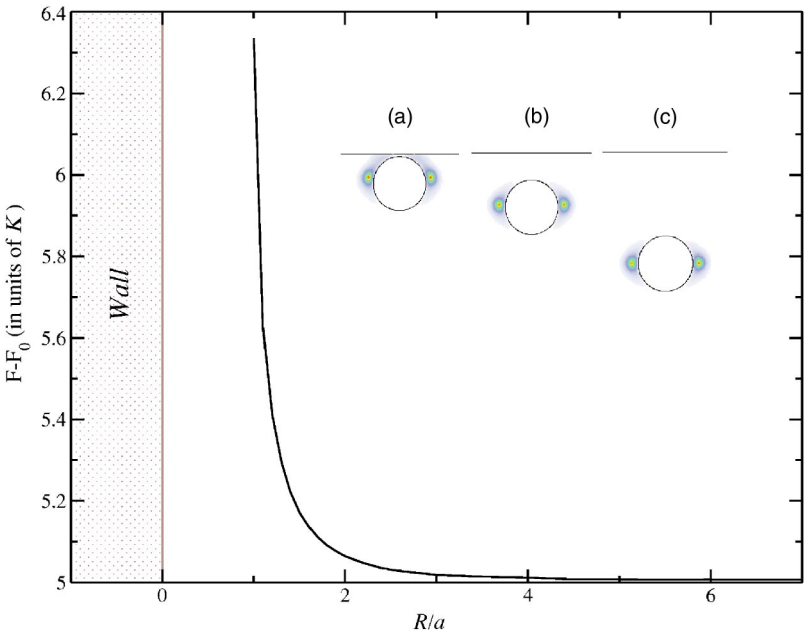

FIG. 1. (Color online) Reduced interaction energy as a function of the distance R from the center of the colloid, of radius a, to the wall. $\overline{F}=F/K$, where $K=2LQ_{bulk}$ is the Frank elastic constant, and F_0 is the Landau–de Gennes free energy of the system without colloid. The inset illustrates the order parameter maps at different R. (a) $R/a=1.1$; (b) $R/a=2.0$; (c) $R/a=4.0$. The nematic order parameter varies between $Q=Q_{bulk}$ (white regions) and $Q=0$ (colored regions).

$$F[Q_{\alpha\beta}, \nabla Q_{\alpha\beta}] = \int_\Omega d^2r \left[-\frac{A}{2}\mathrm{Tr}\{\mathbf{Q}^2\} + \frac{C}{4}\mathrm{Tr}\{\mathbf{Q}^2\}^2 + \frac{L}{2}\nabla_\gamma Q_{\alpha\beta}\nabla^\gamma Q^{\alpha\beta}\right], \quad (1)$$

where we used the one elastic constant approximation. Tr denotes the trace operation, Ω is the area of the 2D system, A and C are bulk constants, and L is the elastic constant. Stability requires $C>0$. In the nematic phase $A>0$ and the equilibrium orientational order parameter is $Q_{bulk}=\sqrt{2A/C}$. For simplicity, we consider strong homeotropic (perpendicular) anchoring meaning that the order parameter at the wall and disk boundary is fixed and equal to Q_{bulk}. The colloid is modeled as a hard disk, and all other colloidal interactions (van der Waals, electrostatic, etc.) are neglected. Thermal fluctuations, also neglected within the Landau–de Gennes description, are expected to be unimportant for the systems considered here: hard surfaces at temperatures well below the NI transition temperature.

We use finite elements with adaptive meshing, as described in Ref. [13], to minimize the Landau–de Gennes free energy functional. Indeed, the major difficulty in the numerical problem stems from the widely different length scales set by the disk or the sculpted wall and the defects. A first triangulation respecting the (predefined) geometrical boundaries is constructed. The tensor order parameter $Q_{\alpha\beta}(\mathbf{r})$ is given at the vertices of this mesh and linearly interpolated within each triangle. The free energy is then minimized using standard methods. The variation of the solution at each iteration is used to generate a new adapted mesh. In the far field $Q_{\alpha\beta}(\mathbf{r})$ varies slowly and the triangles are large. By contrast, close to the defects the tensor order parameter varies rapidly and the triangles are several orders of magnitude smaller. In typical calculations convergence is obtained after two mesh adaptations, corresponding to final meshes with 10^4 points, spanning a region of $20a\times 20a$, and minimal mesh sizes of $10^{-4}a$, close to the defects. The corresponding free energy is given with a relative accuracy of 10^{-4}.

III. FLAT WALL

We start by considering the interaction of a colloidal disk, of radius a, with a flat wall. We assume strong homeotropic boundary conditions at the wall and at the disk's surface, and take the far field $\mathbf{n}_0$ perpendicular to the wall. The order parameter at the wall and at the disk's surface is fixed and is equal to Q_{bulk}.

The fixed homeotropic anchoring at the boundaries reduces the (long-range) flat disk-wall interaction to the interaction between two disks, studied in Ref. [14]. The latter was obtained using an electromagnetic analogy [10] establishing that, at large separations, each disk is accompanied by a pair of defects and behaves as a quadrupole. This still applies to the flat wall system with the result that the long-range disk-wall interaction is repulsive and decays as R^{-4}, where R is the distance between the center of the disk and the wall. However, at short range, nonlinear effects come into play, and the electromagnetic analogy is no longer valid. Moreover, in that region the equilibrium disk-disk interaction spontaneously breaks the flat wall (mirror) symmetry [14] and thus it is no longer useful in this problem. In this regime, we resorted to numerical solutions.

In Fig. 1 we plot the reduced interaction energy $\overline{F}-\overline{F}_0$ as a function of the distance R. $\overline{F}=F/K$, where $K=2LQ_{bulk}$ is the Frank elastic constant, and F_0 is the Landau–de Gennes free energy of the system without colloid. As noted above, the long-range interaction is always repulsive and we find that the repulsion increases as the colloid approaches the wall. This increased short-range repulsion is associated with the strong distortion of the nematic matrix between the (flat) wall and the (curved) disk, due to the competition between the fixed anchoring conditions at the wall and disk surfaces. The distortion of the nematic matrix extends from the wall

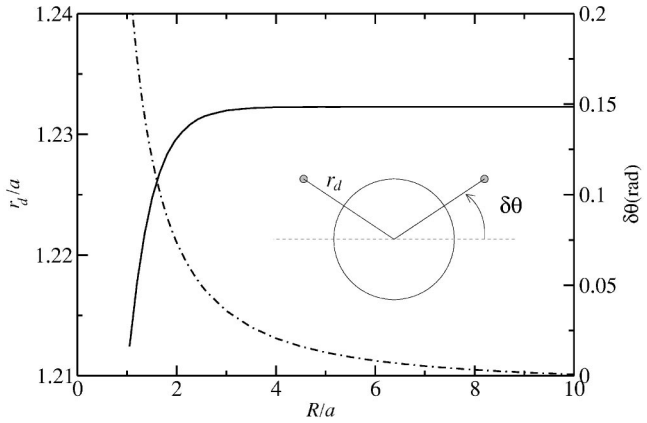

FIG. 2. Defect distance r_d from the center of the disk (continuous line) and defects orientation $\delta\theta$ (dash-dotted line), with respect to their orientation in isolated disks, as a function of R.

up to the line joining the defects and under these circumstances the elastic free energy is minimized if the defects move closer to the wall. As a result the pair of $1/2$ defects surrounding the disk are displaced with respect to their (symmetrical) equatorial position in the isolated disk. This effect is illustrated in the inset of Fig. 1, exhibiting order parameter maps at different disk-wall separations, R. In Fig. 2, we plot the defects orientation $\delta\theta$ with respect to their orientation in isolated disks, as a function of R (see inset for the notation). In addition, the distance of the defects from the center of the disk, r_d/a, decreases at small disk-wall separations, R, as the defects change their orientation.

IV. STRUCTURED WALL

The results of the preceding section indicate that a homeotropic disk is repelled by a hard (homeotropic) wall since the elastic deformation of the nematic matrix increases as the colloid approaches the wall. This situation may be inverted if the director field at the wall resembles the director field close to an isolated disk. In the following we explore this mechanism and determine the conditions under which it is strong enough to overcome the flat wall repulsion.

We consider a sculpted cavity on an otherwise flat wall, as shown in Fig. 3. The cavity is spherocylindrical of radius r and half-length or depth d. The corners are replaced by an arc of circle with radius $a/4$, to avoid large variations in the director field, in the absence of the colloid. Strong homeotropic boundary conditions are set at the wall and at the colloidal surface. The far field $\mathbf{n}_0$ is again perpendicular to the wall.

The image method can no longer be applied and analytical expressions for the long-range interaction between the disk and the cavity are not available in this case. In addition, the nonlinearities that come into play, as the colloid approaches the cavity, are more complex. The free energy is minimized numerically as before, using finite elements with adaptive meshing [13].

We start by considering a very shallow cavity, with $d/a=0.01$. In Fig. 4 we show the disk-wall interaction as a function of the separation R/a for increasing values of the cavity's radius. If the cavity is sufficiently narrow ($r/a<0.25$) the colloid-wall interaction is very similar to the interaction with the flat wall. As the radius of the cavity increases, an attraction with a well defined minimum eventually occurs. The minimum is inside the cavity if the width is larger than the colloidal radius, $r/a>1$.

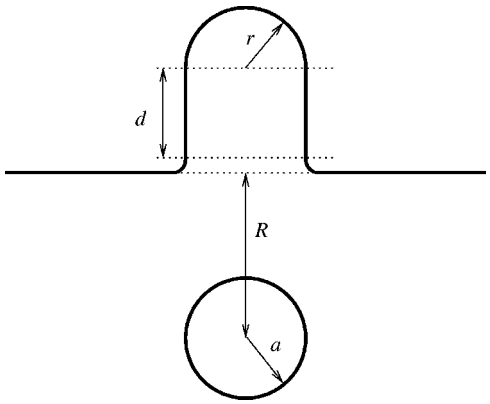

FIG. 3. Structured wall: geometry and notation.

However, if we increase the radius of the cavity well beyond the colloidal size, the attraction becomes very weak. When the radius of the cavity is much larger than a, the interaction between the disk and the structured wall approaches that of the flat wall.

The disk-wall attraction that occurs when the radius of the cavity is of the order of the particle radius is easily understood in terms of the nematic configurations of Fig. 5, where we plot the nematic order parameter maps and the director orientation, for a cavity with $r/a=1.1$ and $d/a=0.01$, and different colloidal separations R. The shape of the cavity is complementary to that of the disk. The distortion due to the homeotropic anchoring at all surfaces is clearly minimized when the particle fills the cavity. In fact, as the colloid approaches the cavity, the two $1/2$ defects move towards the corners and merge with the distorted region of the nematic matrix in the absence of the colloid [see Fig. 5(a)]. Due to

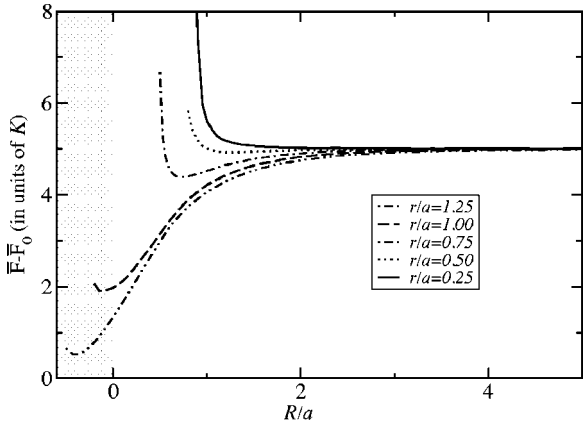

FIG. 4. Reduced interaction energy as a function of the distance R of the center of the colloid to the midpoint of the cavity's entrance for several widths ($r/a=0.25,0.50,0.75,1.00,1.25$). The depth is $d/a=0.01$.

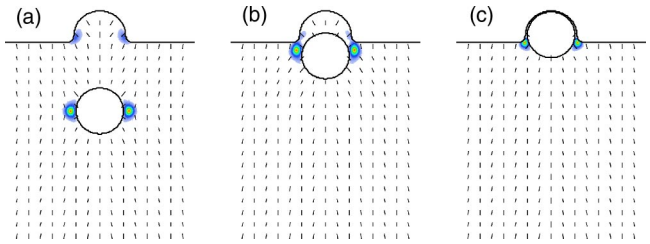

FIG. 5. (Color online) Order parameter maps for a cavity with $r/a=1.1$ and $d/a=0.01$, and different colloidal separations R. (a) $R/a=3.0$; (b) $R/a=0.6$; (c) $R/a=-0.32$. The nematic order parameter varies between $Q=Q_{bulk}$ (white regions) and $Q=0$ (colored regions).

the strong distortion of the nematic matrix at the corners of the isolated cavity, the tensor order parameter decreases in this region, even if we keep $Q=Q_{bulk}$ fixed at the surface. Different surface interactions will lead to different director configurations but for simplicity we restrict the study to strong anchoring conditions.

In Fig. 6 we plot the minimal interaction energy $\overline{F}_{min}-\overline{F}_0$ (left) and the corresponding disk-wall separation R_{min}/a (right) as a function of the radius of the cavity r/a. For small r/a, the disk-wall interaction is repulsive, and the minimal free energy occurs when the colloidal particle is far from the wall, $R\to\infty$. The disk-wall interaction becomes attractive at finite R_{min}/a (corresponding to a critical cavity radius $r_c/a \simeq 0.4$). Beyond this point, the minimal free energy decreases rapidly and reaches its lowest value for a cavity with $r_m/a \simeq 1.1$. The strongest disk-wall attraction occurs for this geometry, and is illustrated in Fig. 5.

In the following we show that the disk-wall attraction, discussed for shallow cavities, may be enhanced by increasing the cavity depth d. In Fig. 7 we plot the reduced interaction energy as a function of the separation R for cavities with different depths d. The cavity radius is $r/a=1.5$ and $r/a=3.0$, on the left and right of the figure, respectively. Increasing d reduces the equilibrium interaction energy by pulling the disk deeper into the cavity. The nematic distortion is decreased and the defects are further localized at the corners leading to a significant reduction in the elastic free energy.

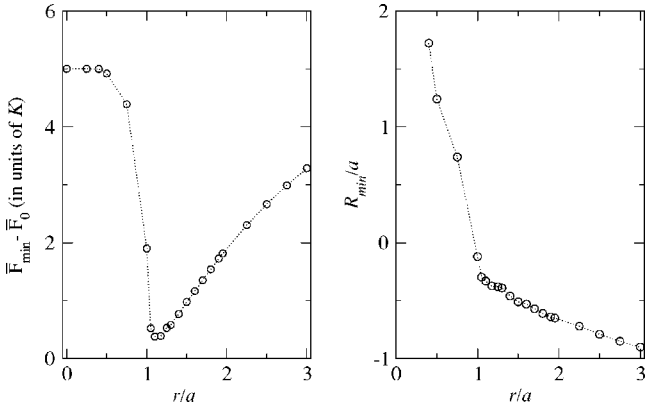

FIG. 6. Minimal interaction energy (left) and equilibrium position R_{min} (right) as functions of the radius of the cavity r/a.

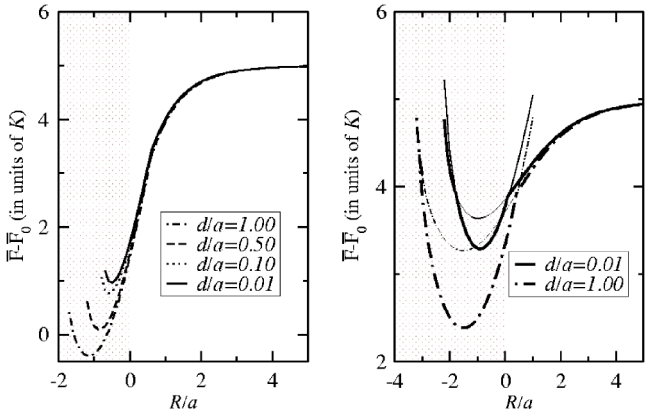

FIG. 7. Left: interaction energy as a function of the separation R for several cavities ($d/a=0.01, 0.10, 0.50, 1.00$) with radius $r/a=1.5$. Right: interaction energy as a function of the separation R for several depths ($d/a=0.01, 1.00$). The radius of the cavity is $r/a=3.0$. The lines in bold correspond to the minimal energy configurations. Thinner lines correspond to metastable solutions.

For cavities with $r/a=3.0$ the analysis revealed the existence of a second (metastable) solution where the defects remain attached to the colloid. This is illustrated in Fig. 7 (right) where we plot the energy of both configurations for two different cavities, $d/a=0.01$ (full lines) and $d/a=1.00$ (dashed lines). The lines in bold correspond to the minimal energy branches.

When $r\sim a$, the disk-wall attraction is enhanced as the depth d increases. A similar effect occurs for wider cavities. However, as was pointed out before, the attraction becomes weaker, and eventually turns into a repulsion as the wall becomes flatter.

The enhancement of the disk-wall attraction occurs only for a limited range of depths. At a certain depth the nematic configuration changes abruptly. In fact, due to the strong homeotropic boundary conditions, there is a critical depth d_c beyond which the stable nematic configuration of the empty cavity exhibits two topological defects (see inset of Fig. 8).

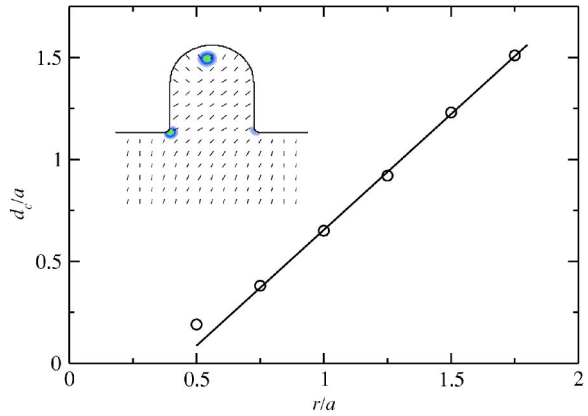

FIG. 8. (Color online) Critical depth d_c as a function of the radius of the cavity. The continuous line is the fit $d_c/a=0.48+1.14r/a$. Inset: Order parameter map for a nematic filled cavity of depth $d\gg d_c$. The nematic order parameter varies between $Q=Q_{bulk}$ (white regions) and $Q=0$ (colored regions).

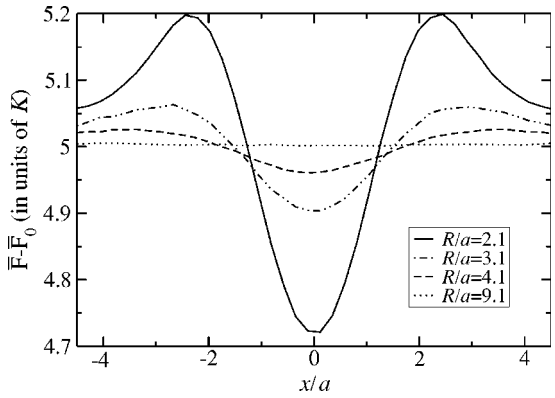

FIG. 9. Reduced interaction energy along four lines parallel to the wall ($R/a=2.1,3.1,4.1,9.1$) as a function of the lateral distance from the cavity x/a. The radius and depth of the cavity are $r/a=1.5$ and $d/a=1.00$, respectively.

One topological defect is inside the cavity, near the cap, while the other is pinned near one of the corners. This broken symmetry configuration is twofold degenerate. Along the cavity's neck the nematic director is almost constant and this configuration will be badly distorted by a colloidal disk. This results in a free energy barrier leading to a strong colloidal repulsion. The barrier will vanish for cavities that are wide enough to allow a smooth deformation of the director field when the colloidal particle is inserted.

Simple dimensional arguments may be used to understand this configurational instability. For smooth deformations, the elastic free energy of the nematic is proportional to Kd/r. By contrast, the free energy of a uniform nematic aligned along the cavity's neck, with two $1/2$ defects placed symmetrically at both ends, scales as, $\pi q^2 K$, the core energy of the defects. Thus, the latter is the equilibrium configuration for sufficiently large d. However, as seen in the inset, at the instability a symmetry breaking transition also occurs and the lower defect is pinned near one corner. In order to ascertain the validity of the simple dimensional arguments we have checked numerically that the energy of the smooth deformation scales with d, while that of the broken symmetry configuration is constant. The critical depths d_c/a were also calculated numerically and are plotted in Fig. 8 as a function of the cavity radius r/a. At large r/a this exhibits the linear relation, $d_c/a=0.48+1.14r/a$.

The results so far considered the interaction between colloidal disks and sculpted walls along the symmetry axis of the cavity (see Fig. 3). In the remaining part of this section we consider the interaction energy along different directions. In Fig. 9 we plot the interaction energy along lines parallel to the wall ($R/a=2.1,3.1,4.1,9.1$), as a function of the lateral distance from the cavity x/a for a cavity with $r/a=1.5$ and $d/a=1.00$. Note that the attraction is limited to a certain angle that depends on the colloidal separation R. Outside that region, the colloid is repelled by the flat wall and by the cavity corners. Indeed, a strong variation of the interaction energy as the disk approaches the corners may be seen in Fig. 9.

The colloid will be trapped by an appropriately sized cavity if, and only if, it is (driven) inside the cavity's "cone" of attraction.

V. CONCLUSIONS

We studied the interaction of a colloidal disk, in a 2D nematic, with a flat wall with strong homeotropic boundary conditions and found that it is purely repulsive and decays at long range as R^{-4}. By sculpting the surface with a cavity that is similar in size and shape to the colloid we found a robust key-lock mechanism, capable of turning the repulsion into an attraction large enough to trap colloidal particles.

This key-lock mechanism is clearly dependent on the geometry of both the colloid and the cavity and its effectiveness for other colloidal shapes will be addressed in future work. Another relevant question that is left open is the existence of a similar effect at soft (deformable) walls. This will allow contact with recent results at NI interfaces where colloids were found to be trapped through a mechanism that is somewhat more complex, since the bending of the interface results from the colloidal interactions [17].

Lastly, we note that the key-lock mechanism has features reminiscent of the process of wrapping colloids by a membrane [20,21]. It is likely that the major factors determining this wrapping process are most simply illustrated for the type of hard structured walls considered in this work. However, a detailed comparison of hard and soft surfaces requires further analysis based on the LdG approach and/or effective Hamiltonian models, in order to assess (among other things) the role of thermal fluctuations.

We end with the remark that our results for the 2D key-lock mechanism are applicable to a particular 3D system, consisting of long rodlike colloids with their major axes parallel to a planar surface. Methods to manipulate such systems have already been developed [22]. Three dimensional effects, such as the biaxiality at the defect cores, are small [23] and thus the key-lock mechanism reported here should be valid for these 3D systems where the non-uniformity is (quasi) two-dimensional.

[1] H. Stark, Phys. Rep. **351**, 387 (2001).
[2] S. Ramaswamy, R. Ninyananda, V. A. Raghunathan, and J. Prost, Mol. Cryst. Liq. Cryst. Sci. Technol., Sect. A **288**, 175 (1996).
[3] P. Poulin, V. Cabuil, and D. A. Weitz, Phys. Rev. Lett. **79**, 4862 (1997).
[4] T. C. Lubensky, D. Pettey, N. Currier, and H. Stark, Phys. Rev. E **57**, 610 (1997).
[5] P. Poulin, H. Stark, T. C. Lubensky, and D. A. Weitz, Science **275**, 1770 (1997).
[6] J.-C. Loudet, P. Barois, and P. Poulin, Nature (London) **407**, 611 (2000).
[7] V. G. Nazarenko, A. B. Nych, and B. I. Lev, Phys. Rev. Lett. **87**, 075504 (2001).

[8] P. Poulin, N. Frances, and O. Mondain-Monval, Phys. Rev. E **59**, 4384 (1999).
[9] S. P. Meeker, W. C. K. Poon, J. Crain, and E. M. Terentjev, Phys. Rev. E **61**, R6083 (2000).
[10] D. Pettey, T. C. Lubensky, and D. R. Link, Liq. Cryst. **25**, 5 (1998).
[11] P. Cluzeau, P. Poulin, G. Joly, and H. T. Nguyen, Phys. Rev. E **63**, 031702 (2001).
[12] P. Cluzeau, V. Bonnand, G. Joly, V. Dolganov, and H. T. Nguyen, Eur. Phys. J. E **10**, 231 (2003).
[13] P. Patrício, M. Tasinkevych, and M. M. Telo da Gama, Eur. Phys. J. E **7**, 117 (2002).
[14] M. Tasinkevych, N. M. Silvestre, P. Patrício, and M. M. Telo da Gama, Eur. Phys. J. E **9**, 341 (2002).
[15] J. Fukuda and H. Yokoyama, Eur. Phys. J. E **4**, 389 (2001).
[16] J. L. West, A. Glushchenko, G. Liao, Y. Reznikov, D. Andrienko, and M. P. Allen, Phys. Rev. E **66**, 012702 (2002).
[17] D. Andrienko, M. Tasinkevych, P. Patricio, and M. M. Telo da Gama, Phys. Rev. E **69**, 021706 (2004).
[18] S. Herminghaus *et al.*, Adv. Mater. (Weinheim, Ger.) **11**, 1393 (1999); F. R. Service, Science **282**, 399 (1998).
[19] P. G. de Gennes and J. Prost, *The Physics of Liquid Crystals* 2nd ed. (Claredon Press, Oxford, 1993).
[20] A. Boulbitch, Europhys. Lett. **59**, 910 (2002).
[21] M. Deserno and T. Bickel, Europhys. Lett. **62**, 767 (2003).
[22] C. Lapointe, A. Hutlgren, D. M. Silevitch, E. J. Felton, D. H. Reich, and R. L. Leheny, Science **303**, 652 (2004).
[23] D. Andrienko, M. Tasinkevych, P. Patricio, M. P. Allen, and M. M. Telo da Gama, Phys. Rev. E **68**, 051702 (2003).